A Monte Carlo Simulation Study of Methane Clathrate Hydrates Confined in Slit-Shaped Pores

ARTICLE *in* THE JOURNAL OF PHYSICAL CHEMISTRY B · FEBRUARY 2012

Impact Factor: 3.3 · DOI: 10.1021/jp205241n · Source: PubMed

THE JOURNAL OF PHYSICAL CHEMISTRY B

Article

pubs.acs.org/JPCB

A Monte Carlo Simulation Study of Methane Clathrate Hydrates Confined in Slit-Shaped Pores

Somendra Nath Chakraborty and Lev D. Gelb*

Department of Materials Science and Engineering, University of Texas at Dallas, Richardson, Texas 75080, United States

Supporting Information

ABSTRACT: Monte Carlo simulations are used to study the structure, stability, and dissociation mechanisms of methane hydrate crystals inside carbon-like slit-shaped pores. The simulation conditions used mimic experimental studies of the dissociation of methane and propane hydrates in mesoporous silica gels (Handa, Y. P.; Stupin, D. *J. Phys. Chem.* **1992**, *96*, 8599). Simulations are performed under conditions of fixed methane pressure and fixed water loading, with the temperature increased in steps, with long equilibrations at each temperature. The initial structures of the confined hydrates are taken to be bulk-like, and pore widths chosen to accommodate integer or half-integer numbers of hydrate unit cells. Density profiles and orientational order parameter profiles are obtained and used to understand the structural changes associated with hydrate dissociation. Three different common water models, SPC/E, TIP4P, and TIP4P/2005, are used and the results compared. For water modeled using either the TIP4P or TIP4P/2005 potentials, dissociation temperatures are depressed proportionally to the inverse pore width, as predicted by the macroscopic Gibbs−Thomson equation. This behavior is observed for pores small enough that only half-cages of the clathrate structure are present. Experimental work has verified Gibbs−Thomson behavior for pores as small as 2 nm (Seshadri, K.; Wilder, J. W.; Smith, D. H. *J. Phys. Chem. B* **2001**, *105*, 2627); micropores of the size studied here have not yet been studied by experiment. Interestingly, the dissociation of hydrates modeled using the SPC/E water potential does not display the predicted pore-size dependence, and the dissociation mechanisms in this model seem to be quite different than those in the TIP4P-type models. In the SPC/E hydrates, with increasing temperature, cage dissocation occurs before methane desorption. In TIP4P-type hydrates, these processes occur either at the same temperature (to within the resolution of this study) or with dissociation occurring at higher temperatures than desorption. These simulations show that a variety of interesting clathrate structures and phase behaviors may be accessed in suitably designed microporous materials, with potentially useful applications in gas storage or separations.

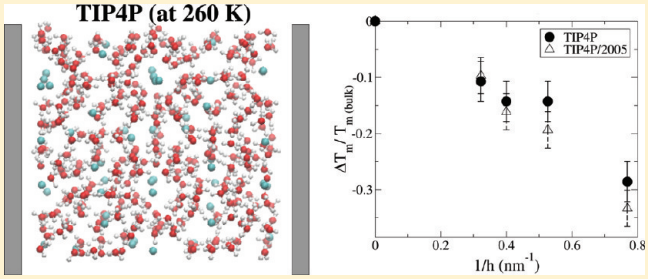

I. INTRODUCTION

Clathrate hydrates are crystalline compounds of water and "guest" molecules, found in nature mainly in permafrost and in the deep ocean regions. The water molecules in these hydrates form cages with nearly spherical cavities, which are occupied by small hydrophobic species such as methane, carbon dioxide, or hydrogen. In these structures, each water molecule participates in four hydrogen bonds (as in ice), and van der Waals interactions between the gas and water molecules help to stabilize the cage structures. Different crystal structures are formed depending on the size of the guest species. The commonly seen crystal structures of clathrate hydrates are cubic (sI), cubic (sII), and hexagonal (sH),[1−5] though hydrates of trigonal (sT) structure have recently been discovered.[6]

Methane clathrate hydrates are of the cubic (sI) type. Each unit cell of the sI crystal is composed of 46 water molecules. These form eight cages, each of which can hold one methane molecule. The actual cage occupancy is a function of temperature and pressure. There are two small pentagonal dodecahedral (5^{12}) cages, each formed by 20 water molecules, and six tetracaidecahedral ($5^{12}6^2$) cages, each formed by 24 water molecules. The average cavity radii of the small and large cages are approximately 4.0 and 4.3 Å, respectively.[3,7]

The phase diagram of hydrates confined in sediments is of considerable interest. It is believed that ∼2.6 × 10^{16} kg of methane are trapped at the ocean floors in this form.[8,9] In coarse-grained sediments (average particle size of a few μm), hydrates form at temperatures and pressures comparable with bulk-phase conditions, but in fine-grained sediments (<1 μm), hydrate formation is inhibited due to capillary effects.[10]

Understanding the thermodynamics and kinetics of the decomposition of confined hydrates is of significant practical importance. Efficient extraction of methane from oceanic deposits will require understanding the phase diagram and stability of these systems with respect to pore size, geometry, and surface chemistry. The possible release of methane from natural hydrates (perhaps due to ocean warming) could be a significant new source of greenhouse gas. Finally, if porous

Received: June 3, 2011
Revised: December 28, 2011
Published: February 9, 2012

materials can be designed such that confinement increases the thermal stability of gas hydrates, such materials could be the basis for high-density storage of hydrogen gas under ambient conditions.[11−13]

Bulk methane hydrates form in the temperature and pressure ranges of approximately 270−285 K and 2−10 MPa, respectively.[1] The methane/water phase diagram displays ice−hydrate−gas and liquid water−hydrate−gas triple lines, which meet at a quadruple point where the hydrate, ice, liquid water, and gas phases are in equilibrium. The quadruple point is located at 272 K and 2.563 MPa.[1] At 273.15 K, the methane hydrate has a density of 0.91 g/cm^3, similar to the density of water ice at this temperature. Ice and methane hydrate differ most significantly in thermal conductivity and thermal expansivity. The interaction between the methane molecules and the water lattice substantially lowers the thermal conductivity and increases the thermal expansion coefficient of the hydrates as compared to ice.[14,15]

The phase diagram of hydrates in pores is significantly different from that of bulk hydrates. Handa and Stupin performed the first detailed measurements of hydrate stability in nanoporous materials, investigating the dissociation of methane and propane hydrates in silica gel with pores of 7 nm average radius.[16] In these experiments, water was first preadsorbed into the silica gel, and the system then exposed to methane gas in order to form the hydrate; the temperature and external methane pressure were simultaneously adjusted to obtain points along the hydrate/liquid/gas triple line. The loading of water in the pores was presumed to remain constant. At any given temperature, the confined hydrates were found to dissociate at pressures 20−100% higher than that found in the bulk. That is, the confined hydrates were less stable at low methane pressures. Also, while in bulk hydrates the slope of the ice−hydrate−gas equilibrium line changes distinctly at the quadruple point, no sharp change was observed in the confined system, so it was not possible to precisely identify a "pore quadruple point". The authors concluded that this behavior was due to the distribution of pore sizes in the material, which would cause the hydrates in different pores to melt over a range of temperatures.

In a different study, Uchida et al. found that in silica glasses with mean pore diameters of 10, 30, and 50 nm, methane hydrates were less stable than bulk hydrates, dissociating at lower temperatures and higher pressures.[17] In particular, they found $\Delta T/T_m \propto 1/d$, where ΔT is the difference between pore and bulk melting temperatures, T_m is the melting temperature of the bulk hydrate, and d is the pore diameter. The experimental protocols used were similar to those used by Handa and Stupin, though the system temperature was increased at a continuous rate of 0.06 K/h, rather than in a stepwise fashion. In later experiments, Uchida et al. obtained dissociation temperatures of methane hydrates in porous glasses with pore diameters between 4 and 100 nm and of carbon dioxide and propane hydrates in 10−100 nm pores.[18] The maximum shifts in the dissociation temperatures were 12.3 K (methane hydrates) in 4 nm pores and 3 and 7 K (carbon dioxide and propane hydrates) in 10 nm pores. The $\Delta T/T_m \propto 1/d$ relationship was applicable to all the confined hydrates.

Seo et al.[19] measured the liquid water−hydrate−gas equilibrium curves for methane and carbon dioxide hydrates in silica gel pores of diameters 6.0, 15.0, and 30.0 nm. This study found, consistent with work described above, that the three-phase equilibrium line shifted to higher pressures relative to the bulk. Seshadri et al. reported the dissociation pressures for propane hydrates confined in silica gel pores of radii 7.5, 5.0, 3.0, and 2.0 nm. The relative increases in dissociation pressures with respect to the bulk were 53−87% for 7.5 nm pores, 79−110% for 5 nm pores, 78−131% for 3 nm pores, and 200−300% for 2 nm pores.[20] These authors also found that the quadruple point temperatures of the confined systems were inversely proportional to pore size. It was pointed out by Anderson et al. that the heating techniques used in all of these measurements affect the dissociation pressures/temperatures of the confined hydrates. They concluded that the heating technique used by Handa and Stupin and by Seshadri et al. provide the more reliable estimates of hydrate dissociation conditions.[21]

The relationship between $\Delta T/T_m$ and the pore size can be understood on thermodynamic grounds. In the limit of large pores, the shift in melting point for a confined single component fluid is given by the Gibbs−Thomson equation

$$\frac{\Delta T_m}{T_m(\text{bulk})} = -2\frac{(\gamma_{ws} - \gamma_{wl})v}{r_{pore}\lambda_{bulk}} = -2\frac{(\gamma_{sl}\cos\theta)v}{r_{pore}\lambda_{bulk}} \quad (1)$$

where T_m(bulk) is the bulk melting temperature, γ_{ws}, γ_{wl}, and γ_{sl} are the wall−solid, wall−fluid, and solid−fluid surface tensions, v is the molar volume of the liquid, λ_{bulk} is the latent heat of melting, and r_{pore} is the pore width. The second equality results from the use of Young's equation for the contact angle θ at a solid−liquid−wall interface. For $\gamma_{ws} > \gamma_{wl}$ (or, equivalently, $\cos\theta > 0$), the melting temperature in a pore is reduced relative to the bulk. This condition may be expected to hold in many cases but especially when the surface of the porous material is rough or otherwise incompatible with the preferred surface structure of the solid phase.

In the case of confined hydrates, experiments suggest that a layer of liquid water separates the solid hydrate from the pore walls even under conditions where the hydrate is stable.[16] One therefore assumes that the hydrate is fully nonwetting and $\cos\theta = 1$. The only interfacial tension then required is that of the hydrate−liquid water interface, γ_{sl}.

Clarke et al.[22] used this approach to interpret the experimental results of Handa and Stupin[16] but used the vapor−liquid interfacial tension of water, 72 mJ/m^2, in place of the hydrate−liquid tension. Good qualitative agreement was achieved, but positive deviations of up to 15% (for methane) and 29% (for propane) in predicted hydrate dissociation pressures were found. Henry et al.[8] assumed that the hydrate−liquid water surface energy was equal to that of the ice−liquid water interface value of 27 mJ/m^2. Although this was a physically more realistic model than that of Clarke et al., it still resulted in an overestimate of the slope of the $P-T$ curve for this system. Wilder et al.[23] also used 27 mJ/m^2 for the hydrate−liquid surface tension but modified the calculations to incorporate a broad pore size distribution and successfully reproduced the results of both Handa and Stupin[16] and Seshadri et al.[20] Seo et al. used a smaller value for the hydrate−liquid water surface tension (17 mJ/m^2, as suggested by Uchida et al.[18]) and obtained good agreement with their own experimental data.[19] Klauda and Sandler modeled the Handa and Stupin system using an alternative approach based on fugacities and also incorporating a broad pore size distribution and obtained reasonable agreement[24] with measured data.

Molecular simulations of confined hydrates can provide a microscopically detailed picture of the behavior of these systems, and help to understand their thermophysical properties and phase stability. In simulations, the pore size, geometry, and surface interactions can be independently and precisely controlled, so that effects due to these different aspects of the pore structure can be resolved. Computer simulations have been very successful in developing a detailed understanding of capillary phenomena and confinement-induced shifts in freezing of simple liquids.[25,26] Molecular simulations have been applied to bulk hydrates by many groups,[14,15,27−30,30−36] but confined hydrates have not so far been treated using these methods.

Prior simulation studies of the bulk phase behavior of methane hydrates are used as reference data for this work. There have been a number of such studies.[37−41] Three-site (SPC/E)[42] or four-site (TIP4P)[43] rigid water models have generally been used, despite the fact that these models were developed for use in liquid-state simulations at or near ambient conditions, and their ability to describe ice phases and freezing transitions is somewhat limited. Methane is usually modeled using either the OPLS-UA or OPLS-AA force fields; all of these potentials are described in the next section.

The SPC/E model of water has a melting point of 215 K at ambient pressure, the TIP4P model has a melting point of 232 K,[44] and the TIP4P/2005 model, 250 K,[45] the closest to the experimental value of 273 K. The TIP4P model reproduces the experimental phase diagram of water better than the SPC/E model.[44] Forrisdahl et al. used molecular dynamics in the *NVT* ensemble to investigate the melting of sI hydrates modeled with the SPC, SPC/E, and TIP4P potentials for water and the OPLS-UA and Tse potentials for methane.[37] Starting at 270 K, the temperature was raised in 5 K steps, every 5 ps. All the hydrates dissociated between 350 and 400 K. To more precisely locate the melting temperatures, longer simulation times were used. At 330 K, the SPC/OPLS hydrate was stable over an 11 ns simulation, but at 340 K, it melted within 1 ns, suggesting that this temperature is above the thermodynamic melting point. Rodger et al. simulated methane hydrates using SPC water and single-site LJ methane. The model hydrate was found to be stable up to 270 K at 1 MPa and up to 280 K at 100 MPa .[41] Mastny et al. directly simulated the coexistence of the hydrate, water, and gas phases using molecular dynamics.[38] They set up a large cubic simulation box containing three phases in four layers—the hydrate phase, two water phases, and methane gas—such that the hydrate only directly contacted the water. The TIP4P water model and OPLS-AA methane model were used, with water−methane LJ interaction parameters obtained from *ab initio* calculations by Sun and Duan.[39] The melting temperature of the sI hydrate was found to be between 287 and 302 K at 400 bar. Sizov and Piotrovskaya used grand canonical ensemble simulations of bulk sI methane hydrate (modeled with SPC/E water and OPLS-UA methane) to show that for methane occupancies below 40% the hydrate structure is substantially degraded. The melting temperature of the hydrate was reported to be in the range 230—235 K at an applied methane pressure of 3 bar.[40]

II. SIMULATION DETAILS

In the present work, the dissociation of sI methane hydrates in slit-shaped pores of several sizes is investigated using Monte Carlo simulations. We here discuss the simulation conditions, pore model, and preparation of the initial confined hydrate structures.

A. Ensemble and Simulation Conditions. All simulations are performed in the constant (N_{H_2O}, μ_{CH_4}, V, T) ensemble. The number of water molecules in the pore is kept constant, while the amount of methane present fluctuates about an average value controlled through its chemical potential. These conditions are chosen to mimic the experimental setup of Handa and Stupin,[16] in which the amount of water (preadsorbed into the pores) is kept fixed while the methane pressure and system temperature are controlled variables. For each system, an "isobaric" series of simulations was performed at increasing temperatures and at constant external methane pressure. At every point along each isobar, we obtain the equilibrium methane loading, as well as the density profiles of water and methane across the pore, in order to understand structural changes in the hydrates and locate dissociation transitions; simulation snapshots are also used in this regard. Profiles of a local orientational order parameter are also used to understand the structure of water in these systems. Calculations are repeated with three different water models, SPC/E,[42] TIP4P,[43] and TIP4P/2005,[45] in order to identify any dependence of confined hydrate behavior on the choice of water model. This simulation protocol does not yield a true equilibrium transition temperature but instead the limit of thermal stability of the confined clathrate under quasi-equilibrium conditions, analogous to the superheating branch of a freezing/melting hysteresis loop.

Note that a single thermodynamic pressure is not well-defined inside a porous (or otherwise inhomogeneous) system. While the external methane pressure can be used to specify the state point inside the pore (the bulk methane pressure and chemical potential are interconvertible through the equation of state), this does not mean that the adsorbed fluid need have properties similar to its bulk counterpart at the same temperature and "pressure", and in general, this will not be the case, especially for pores in the nanometer and subnanometer size range.

B. Interaction Potentials for Water and Methane. The water models used differ as follows: SPC/E is a three-site model, in which electrostatic interaction sites are located on the oxygen atom and hydrogen atoms, and a single Lennard-Jones (LJ) interaction site is placed on the oxygen atom. The hydrogen atoms have charges of +0.4238e, and the oxygen atom has a charge of −0.8476e. The positive charges are located at a distance of 1.0 Å from the oxygen atom such that the H−O−H angle is 109.47°. In the four-site TIP4P model, positive charges are again located on the hydrogen atoms, with the negative charge of −1.04e not located on the oxygen atom but 0.15 Å toward the hydrogens along the H−O−H angle bisector. The single LJ interaction site is again centered on the oxygen atom. The O−H distance is 0.9572 Å, and the H−O−H angle is 104.52°. The TIP4P/2005 water model is a reparameterization of the TIP4P model where the negative charge has a value of −1.1128e and the distance from the negative charge to the oxygen atom is increased slightly, to 0.1546 Å. In a recent study, the TIP4P/2005 model was used to obtain the excess chemical potential of methane in water over a broad range of temperatures.[46] For CH_4, we have used a single-site LJ model with OPLS-UA parameters.[47] The potential parameters and ice melting points of all the models are given in Table 1. Interactions between methane and water were entirely of the LJ type, with parameters obtained via the Lorentz−

Table 1. Potential Parameters Used in the Simulations[a]

model	q	σ (nm)	ϵ/k_B (K)	T_m (K)
SPC/E	−0.8476	0.3166	78.23	215
TIP4P	−1.0400	0.3154	78.00	232
TIP4P/2005	−1.1128	0.3159	93.20	250
Methane		0.3730	147.5	
Carbon		0.340	28.0	

[a]The melting temperatures of the water models at 1 bar are also given.[44]

Berthelot combining rules,[48,49] which have previously been reported to be reasonably accurate in describing methane−water interactions, though do give rise to a small systematic deviation in the excess chemical potential of aqueous methane at infinite dilution.[50]

C. Pore Model. Following many previous studies of solid phases and melting transitions in pores,[51−53] we consider here clathrates confined between smooth parallel surfaces. This "slit pore" model is parametrized so as to represent the typical pores found in activated carbon materials, consisting of the space between separated stacks of graphene sheets. The z axis is taken normal to the pore surfaces in the coordinate system used. Periodic boundary conditions are applied in the x and y directions, mimicking an infinite slit pore geometry. The interactions of each pore wall with adsorbed molecules are given by the Steele 10−4−3 potential:[54]

$$u_{sh}(z) = 2\pi\rho_s\epsilon_{sh}\sigma_{sh}^2\Delta\left[\frac{2}{5}\left(\frac{\sigma_{sh}}{z}\right)^{10} - \left(\frac{\sigma_{sh}}{z}\right)^4 - \left(\frac{\sigma_{sh}^4}{3\Delta(z+0.61\Delta)^3}\right)\right] \quad (2)$$

where ρ_s is the number density of carbon atoms in the graphitic planes, Δ is the layer spacing in graphite, and ϵ_{sh} and σ_{sh} are the Lennard-Jones interaction parameters between the carbon atoms of the wall and components of the adsorbed hydrates. Here, z measures the distance of an adsorbate atom from the topmost carbon layer; in the slit pore geometry, the total potential due to the adsorbent on the adsorbing fluids is the sum of interactions with the top and bottom walls of the pore. We note that the Steele potential omits any description of the lateral variation in potential due to the atomic nature of the pore surface, but that this is quite small for graphitic carbon and likely not significant at the temperatures considered. The carbon walls interact with the LJ sites (effectively, oxygen atoms) of the water molecules. Lorentz−Berthelot combining rules are used to obtain ϵ_{sh} and σ_{sh}; ϵ and σ parameters for carbon are given in Table 1.

D. Hydrate Structure Generation. The bulk hydrate crystal structure is "proton disordered", has zero dipole moment, and follows the ice rules.[55] The method proposed by Buch et al. was used to generate proton disordered sI bulk methane clathrate structures as follows:[56]

(1) A rectangular unit cell of 11.877 Å is constructed, and oxygen atoms are placed at coordinates obtained from single crystal X-ray diffraction studies.[57]
(2) One hydrogen atom is assigned to each pair of neighboring oxygen atoms and placed on the O−O vector 1.0 Å from one of the oxygen atoms, chosen randomly. After this procedure, each oxygen atom is bonded to anywhere between zero and four hydrogen atoms.
(3) A stochastic algorithm is then applied to correct the initial placement of hydrogen atoms. A pair of neighboring oxygen atoms is picked at random and the hydrogen atom associated with this pair moved to the other oxygen. The move is accepted with probability 1 if the difference between the coordination numbers of the two oxygen atoms decreases. The move is accepted with probability 0.5 if the difference in coordination numbers does not change, and the move is rejected if the difference increases. 5000 such moves are performed.
(4) The dipole moment of the accepted configuration is then computed.

This procedure is repeated 100 000 times, from which the configuration with the smallest dipole moment is selected for use in the construction of initial configurations for the confined hydrate simulations.

E. Confined Hydrate Structure. Determination of the thermodynamically stable hydrate structure inside small pores is extremely difficult, more so even than the general problem of prediction of bulk crystal structures of molecular species. The presence of the walls means that the repeat unit of the confined crystal must be as large (in at least one dimension) as the pore width and therefore contains more molecules than the corresponding bulk unit cell for all but the narrowest pores. Experimental ^{13}C NMR results have shown that methane hydrates formed in 6, 15, 30, and 100 nm silica gels have the same structure as the bulk hydrate,[19,58] although the detailed structure of the hydrate near the pore wall in these systems is not known; since only a very small fraction of the hydrate in such pores is in contact with the surface, any differences in this region are lost when averaging over the sample. Nevertheless, for the purpose of generating initial molecular configurations, we assume that the confined hydrate structure is bulk-like and, furthermore, that the hydrate crystal is aligned with one (cubic symmetry) axis parallel to the z axis of the simulation cell. That is, the lowest-index planes of the clathrate crystal will be oriented parallel or perpendicular to the planar cell walls. The simulation cell is chosen to be twice the length of the bulk unit cell in the x and y directions; the simulation cells all measure $23.754 \times 23.754 \times h$ Å^3, where h is the distance between the carbon surfaces. h is taken to be $n \times 11.877$ Å $+ 2.0\sigma$, where n is some number of unit cells of hydrate and $\sigma = \sigma_{sh} = \sigma_{wall-CH_4}$. Four different values for n are used, 0.5, 1.0, 1.5, and 2.0, giving pore widths that can accommodate integer or half-integer numbers of hydrate unit cells. The corresponding wall-to-wall spacings are 13.116, 19.007, 24.9455, and 30.884 Å, respectively.

To prepare an initial configuration, a bulk unit cell is generated as described above and then replicated twice in the x and y directions, and several times in the z direction. The cell is positioned "over" the pore, and molecules which overlap the pore material are removed. Even with the geometric assumptions described above, there are many possible ways to position the hydrate crystal over the simulation cell. These correspond to different translations, or "offsets", in the z direction (translations in the x and y directions are irrelevant due to the use of periodic boundary conditions.) We have chosen to focus on offsets where the hydrate surfaces in contact with the two pore walls are the same. Under this restriction, in the $n = 1.0$ and $n = 2.0$ pore sizes, there are two possible offsets,

which differ by a 1/2 unit cell translation in z, as shown for the n = 2.0 case in Figure 1. In each case, we refer to the two

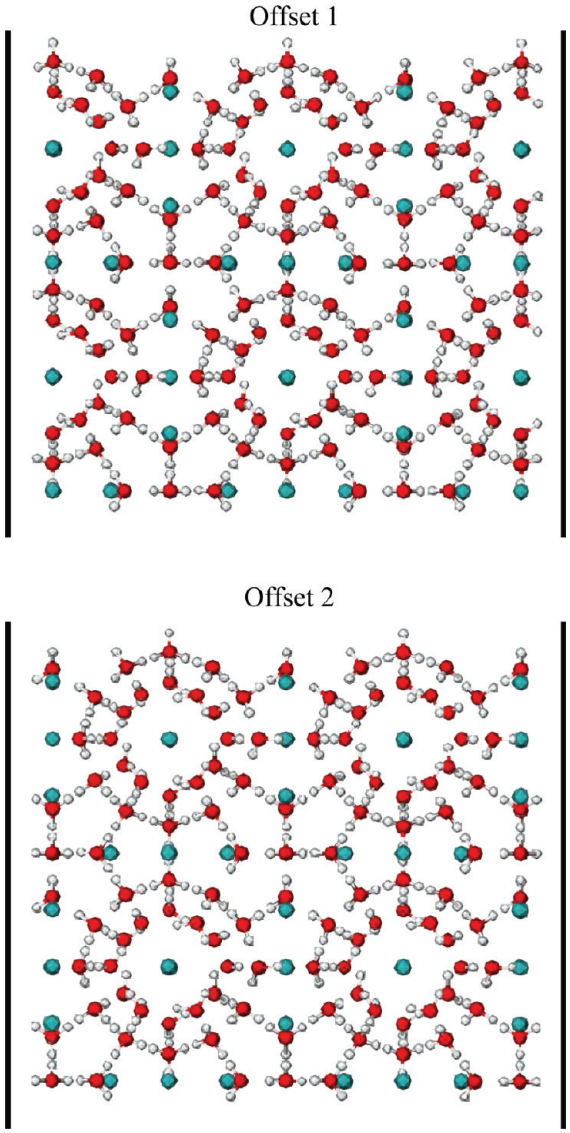

Figure 1. Ideal hydrate structures in the 2.0 u pore. The two "offsets" differ only by a translation of 1/2 unit cell edge length but present significantly different crystal planes to the pore walls. Methane molecules are cyan spheres, oxygen are red, and hydrogen are white.

structures as "offset 1" and "offset 2", and consider both in the simulation study. The difference between the two offsets is somewhat subtle. Both offsets present 12 methanes against the wall, with eight in bisected $5^{12}6^2$ cages and four in bisected 5^{12} cages. The 5^{12} half-cages, however, are cut along perpendicular axes in the two offsets, and because this structure has 5-fold symmetry, these are not equivalent. We also note that the randomized hydrogen-bonding structure leads to additional differences in the orientation of O−H bonds near the surface between the opposing faces for a given offset, and between the different offsets. In the n = 0.5 and n = 1.5 pore sizes, the hydrate crystal planes in contact with the pore walls are necessarily different. In these cases, only a single offset is considered, such that one of the contact planes is the same as that in the (integer n) "offset 1" structures and the other is that in the "offset 2" structures. In total, we simulate six different pore hydrate systems, referred to as "0.5 u", "1.0 u, offset 1", "1.0 u, offset 2", "1.5 u", "2.0 u, offset 1", and "2.0 u, offset 2".

F. Monte Carlo Simulations. Simulations are performed in the (μ_{CH_4}, N_{H_2O}, T, V) ensemble. The number of water molecules (N_{H_2O}) inside the pore is kept fixed, while the amount of methane can fluctuate. We note that specification of the thermodynamic state point in this way for a system of two components permits the presence of up to two phases at equilibrium. The chemical potential corresponding to a specified methane gas pressure is obtained from separate grand canonical Monte Carlo simulations of bulk methane. We report the simulation results in terms of this pressure, for comparison with experimental work.

Simulations are performed in isobaric (constant methane pressure) "series", starting at a low temperature and increasing the temperature in steps of 10 K. At each temperature, the system is fully equilibrated, and the final configuration at each temperature is used as the initial configuration for the next. The starting configuration for each series is obtained by equilibrating at the lowest temperature an ideal hydrate structure as prepared above. Under almost all the conditions studied, these initial configurations are well-structured hydrate crystals with cages fully occupied. For each water model, isobaric series were run at 1, 10, and 100 bar, with the temperature scanned between −20% and +20% of the bulk melting temperature.

In previous Monte Carlo simulations of hydrates in the bulk phase, authors used simulation protocols that differed substantially in the numbers of moves performed and other details. For simulation domains containing 8 unit cells of the sI hydrate structure, prior studies have used as few as 10^7 MC trial moves per state point[40] and as many as 2×10^8 moves;[34] another study of a system containing 64 unit cells was run for 10^9 MC moves per state point.[52] In simulations of 2.0 u, 1.5 u, and 1.0 u hydrates (containing between 4 and 8 unit cells' equivalent material), we have equilibrated each state point for 10^8 moves, after which data were accumulated for another 10^8 moves. For the 0.5 u hydrates, each state point was equilibrated for 5×10^8 moves, and data accumulated for another 5×10^8 MC moves. The total energy and methane adsorption were monitored at each state point in order to ensure equilibration. Inspection of these data, a selection of which are given in the Supporting Information, indicated that these runs were of sufficient length to obtain equilibrated data of reasonable quality. On an Intel Q9400 processor (2.66 GHz), the time required to complete 10^8 MC moves was approximately 44 h in 2.0 u hydrates, 33 h in 1.5 u hydrates, 24 h in 1.0 u hydrates, and 15 h in 0.5 u hydrates. These were long simulations, with most series taking approximately 30 days to complete.

The MCCCS Towhee software package was used for all the simulations.[59] Four types of moves were used: (i) translational moves for water and methane, (ii) rotational moves for water, and (iii) insertion and (iv) deletion moves for methane. The fractions of trial moves were kept at 30, 40, and 30% for translations, rotations, and insertions/deletions, respectively. The target acceptance probabilities of translational and rotational moves were kept at 0.5. The maximum translational and rotational displacements were initially set to 0.25 Å and 3° and as simulations progressed were adjusted to give the desired target acceptance rate. No cluster moves or insertion-bias sampling techniques were used. Since nearly all state points simulated were above the critical temperature of methane, no

dx.doi.org/10.1021/jp205241n | J. Phys. Chem. B 2012, 116, 2183−2197

capillary condensation was expected (or observed) in these simulations. Coulombic interactions were calculated using three-dimensional Ewald summation. LJ interactions were cut off at 9 Å in all the simulations, and bulk-type long-range corrections were used. These conditions correspond not to an isolated pore system but to a "stack" of identical pores, which is a reasonable picture of a high-surface area carbonaceous material.[60,61] The pores are not separated by additional vertical distance, and so pore walls are shared by their periodic images in the z directions. The differences between the simulated system, an isolated "single" pore, and a more realistic model material are nonetheless largely inconsequential, because the net interactions between molecules in one pore and the next are extremely weak and unlikely to influence the observed behavior at the temperatures considered.

G. Analysis. At each state point, 500 statistically independent configurations are collected during the data-accumulation phase, which are used for all subsequent analyses. Quantities measured include the amount of methane adsorbed per unit area of pore, the density profiles of water and methane, and the bond-orientational order parameter profiles of water.

The amount of methane adsorbed per unit area of pore is given in units of molecules/nm^2 and computed as

$$n_{CH_4} = \frac{\langle N_{CH_4} \rangle}{L_x L_y} \tag{3}$$

where $\langle N_{CH_4} \rangle$ is the ensemble average number of adsorbed methane molecules and L_x and L_y are the lengths of pore in the x and y directions, respectively. Uncertainties in n_{CH_4} are computed using block averaging[62] and in all loading data plots are smaller than the symbols used.

The methane and water density profiles in units of molecules/nm^3 are computed as

$$\rho_X(z) = \frac{\langle N_X(z, z + \Delta z) \rangle}{L_x L_y \Delta z} \tag{4}$$

where $X = H_2O$ or CH_4 and $\langle N_X(z, z + \Delta z) \rangle$ is the ensemble average number of H_2O/CH_4 molecules located between planes at z and $z + \Delta z$. In the case of water, oxygen atom positions are used to locate each molecule.

The W_4 bond-orientational order parameter introduced by Steinhardt et al.[63] is used to characterize the ordering of water in the confined clathrates. W_4 is the sum over certain spherical harmonics of the vectors connecting the oxygen atom in one water molecule with those of its nearest neighbors. We construct an order parameter profile $W_4(z)$ by averaging W_4 over the water molecules lying in thin slabs between z and $z + \Delta z$, similar to the density profiles defined above. W_4 was used in a previous study of nucleation phenomena in CO_2 hydrates,[52] in which the average values in bulk sI carbon dioxide clathrate and in liquid water at 220 K and 4 MPa were found to be −0.15 and 0.0, respectively.

III. RESULTS AND DISCUSSION

Results obtained with each water model are discussed as a group, with selected data presented and analyzed in detail. The temperatures of hydrate dissociation at each pressure are then gathered into phase diagrams and compared.

A. TIP4P Hydrates. Series for each of the four TIP4P hydrates (2.0, 1.5, 1.0, and 0.5 u) were run at 1, 10, and 100 bar. All simulations were started at 180 K, and the hydrates were heated until they dissociate, which in all cases occurred by 310 K. At 180 K, all the hydrates were stable and each of the cages occupied by one methane molecule. As the hydrates are heated, methane desorption occurs, sharply in some systems and more gradually in others. Eventually, the hydrates decompose. Some methane is present even after decomposition, which gradually desorbs with further heating.

Methane loadings vs temperature from these simulations are shown in Figure 2. In the 2.0 u pore (Figure 2a) at the lowest pressure of 1 bar, significant desorption begins at 180 K and proceeds gradually, with nearly all the methane gone by 280 K. Actual hydrate decomposition, however, occurs between 250 and 260 K. That is, microscopic analysis of density and order-parameter profiles (discussed below) shows that the characteristic hydrate structure is well-formed at 250 K but absent at 260 K. At 10 and 100 bar, the 2.0 u hydrates display only very limited desorption at low temperatures, followed by sharper drops at higher temperature. These occur over a range of about 20 K and correspond to decomposition of the clathrate structure. In the 1.5 u pore, Figure 2b, sharp decreases in methane loading with increasing temperature occur at all pressures, over temperature ranges corresponding to hydrate dissociation. Decomposition and desorption occur at lower temperatures in the 1.5 u system than in the 2.0 u system. Loading data in the 1.0 u pore (Figure 2c) are very similar to those for the 1.5 u system but shifted to slightly lower temperatures. Similarly, loading data in the 0.5 u pore (Figure 2d) are similar to those in the 1.0 u pore but shifted to yet lower temperatures. In the 0.5 u pore at the highest pressure (100 bar), decomposition occurs between 220 and 230 K, coincident with the sharpest reduction in methane loading. At lower pressures, however, the hydrate structure is already decomposed at 220 K (10 bar) or 200 K (1 bar), just before the sharp methane desorption.

In all pore sizes, at the highest pressure (100 bar), very little methane desorption occurs until near decomposition. In addition, the amount of methane remaining in the pore after collapse of the clathrate structure is quite substantial at high pressure, nearly half that at "full" loading in the same systems. Finally, only in a single system, the 100 bar series in the 1.0 u pore, is any significant difference observed between the two offset structures, with desorption and decomposition occurring in the offset 2 structure approximately 10 K higher than in the offset 1 structure.

Figure 3 shows density and order parameter profiles in the 2.0 u offset 1 TIP4P hydrate at 10 bar and 260, 270, and 280 K. This is the temperature range over which n_{CH_4} falls significantly in Figure 2a. The methane density profiles are shown in Figure 3a. The sharp peaks in methane density are centered in the water cages (see Figure 1). All the peak heights decrease slightly between 260 and 270 K (corresponding to a small reduction in total loading), but between 270 and 280 K, the center of the pore is evacuated by methane, with sharp peaks remaining only close to the walls.

The density profile of the water molecules at 270 K, shown in Figure 3b, exhibits a series of peaks corresponding to the locations of the oxygen atoms in the hydrate structure. In a defect-free bulk hydrate, the average value of the W_4 orientational order parameter is −0.15, as discussed previously. In the confined hydrate system at 270 K, we obtain a complicated W_4 profile with values varying between −0.075 and +0.075. The more negative values are seen in the center of the pore, and correspond to water molecules in well-ordered cages.

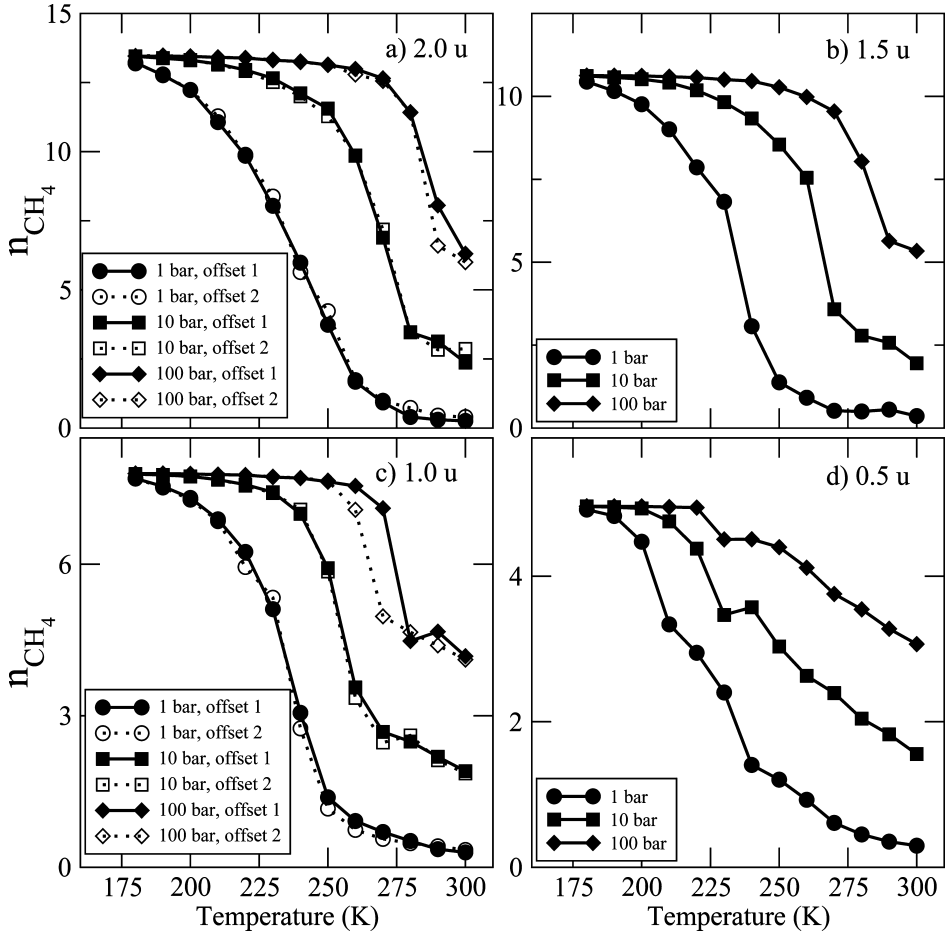

Figure 2. Methane loading data in systems modeled using the TIP4P potential. Methane loading per unit area of pore (n_{CH_4}), with increasing temperature, at constant pressure. Data shown for three pressures, 1, 10, and 100 bar, in six systems: (a) 2.0 u (offset 1 and 2), (b) 1.5 u, (c) 1.0 u (offset 1 and 2), and (d) 0.5 u. Statistical uncertainties in all data are smaller than the symbols used.

Positive W_4 values are seen in the center of the pore only at positions of very low average water density, and correspond to displacements of water molecules away from their sites in the crystalline hydrate lattice structure. Nearer to the walls, the W_4 profile is generally positive but still shows some oscillatory structure. The presence of the walls interrupts the stability of the hydrate crystal, and water molecules in this region are more rotationally and translationally labile than those in the interior of the pore.

The structure in the water profiles disappears more or less completely by 280 K (Figure 3c). There is no crystalline order present at this temperature, which corresponds to the end of the rapid decrease in n_{CH_4} seen in Figure 2a; by this point, the hydrate structure has completely collapsed, with the remaining methane adsorbed at the pore walls. The relatively smooth density profiles in the center of the pore are consistent with liquid-like behavior at this temperature. A typical water density of 1 g/cm^3 corresponds to 33.46 molecules/nm^3 (the units used in these plots), so that the density of water in the center of the pore is close to that of the corresponding bulk liquid. Note that, because water in the hydrate has a lower density than in the liquid phase, there is insufficient water present to fill the entire pore to this density; instead, less water is present at the pore walls, permitting the adsorption of the excess methane seen in Figure 3a.

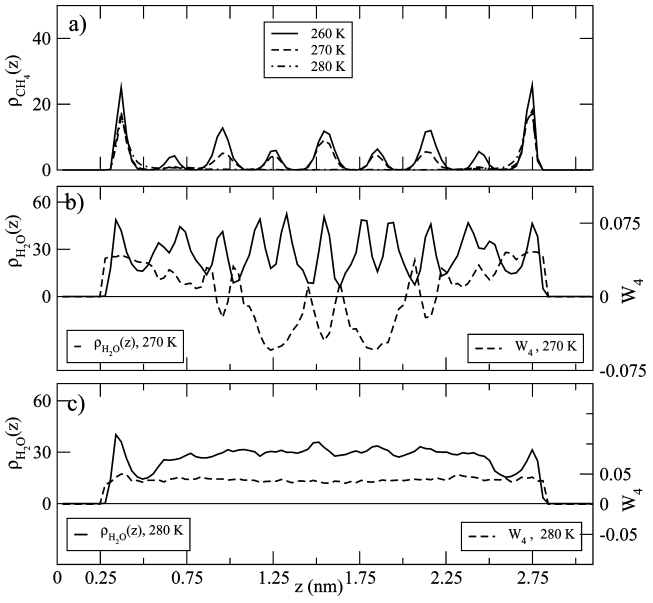

Figure 3. Density and order parameter profiles in the 2.0 u (offset 1) TIP4P hydrate at 10 bar: (a) methane density profiles 260, 270, and 280 K; (b, c) density and order parameter profiles of water at (b) 270 K and (c) 280 K.

dx.doi.org/10.1021/jp205241n | J. Phys. Chem. B 2012, 116, 2183–2197

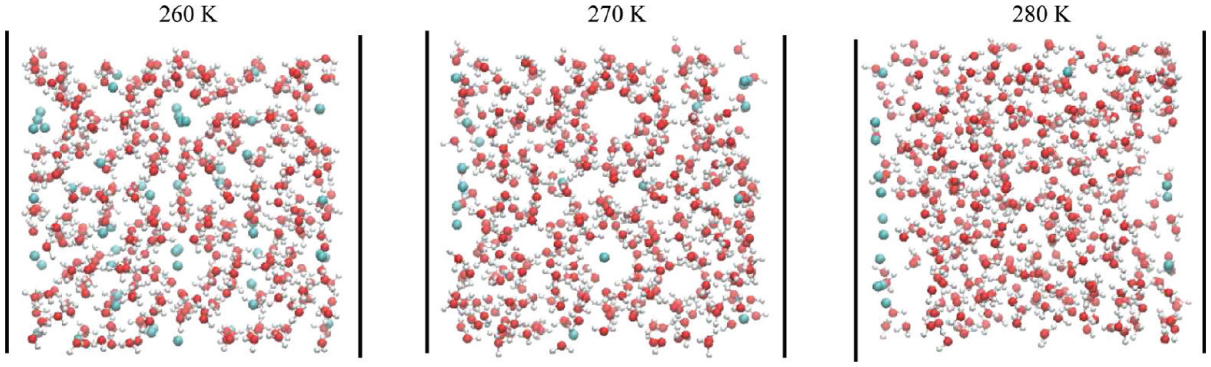

Figure 4. Simulation snapshots of the 2.0 u (offset 1) TIP4P hydrate at 10 bar and at 260, 270, and 280 K. The color scheme is the same as that in Figure 1.

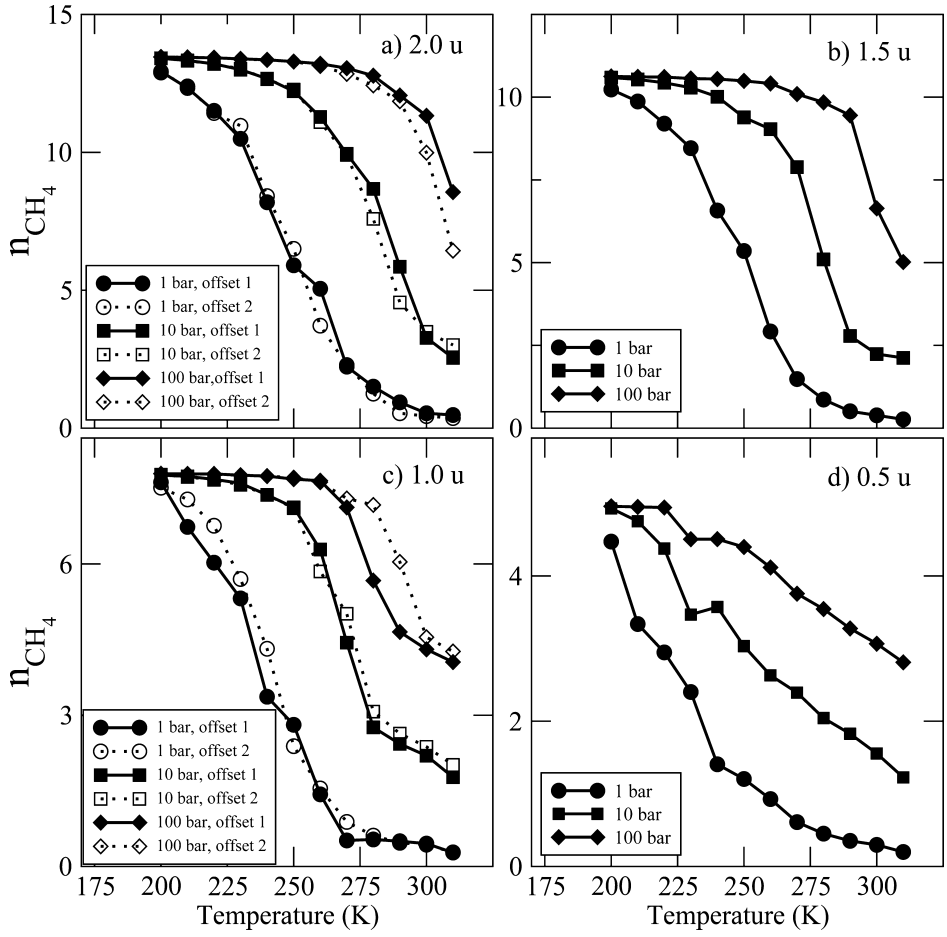

Figure 5. Methane loading data in systems modeled using the TIP4P/2005 potential; details as in Figure 2.

For further confirmation of this picture, simulation snapshots of this system at 260, 270, and 280 K are shown in Figure 4. The hydrate structure is clearly well-formed and fully occupied at 260 K. At 270 K, some empty water cages are visible. At 280 K, there is no visible order in the water structure, and methane is present only near the pore walls. It is clear that in this system as the temperature is increased methane desorbs first, followed by cage dissociation. That is, in most cases, the equilibrium methane loading is significantly reduced at temperatures below the decomposition temperature of the confined clathrate. Similar behavior is observed in other pore sizes as well; this therefore appears to be a feature of the water model, rather than of the 2.0 u pore system. Empty cages have likewise been observed in simulation studies of stable and metastable bulk hydrates.[64] We reiterate that these are (at least on simulation-accessible time-scales) quasi-equilibrium data; describing the kinetic process of hydrate dissociation is not achievable by (grand canonical) Monte Carlo or similar methods but would instead require either molecular dynamics simulations of hydrates confined in finite-length, open-ended pores, or possibly adaptation of the "dual-control-volume grand canonical molecular dynamics" method to this system.[65]

Returning to the 1.0 and 0.5 u isobar data of Figure 2c and d, this mechanism of desorption followed by hydrate structure decomposition affords a possible explanation for the small rises in n_{CH_4} observed in the "offset 2" structures at both 10 and 100

dx.doi.org/10.1021/jp205241n | J. Phys. Chem. B 2012, 116, 2183–2197

bar (1.0 u pore) and at 10 bar (0.5 bar). As explained above, collapse of the clathrate cages creates empty space by the pore walls in which further methane adsorption can take place. Because the adsorbed fluids interact with both pore walls, the depth of the adsorbing potential at the walls increases as the pore is narrowed.[53] Therefore, one expects more substantial methane adsorption at the walls in the narrower pores, which is consistent with the observation of small increases in loading after clathrate collapse in those systems.

B. TIP4P/2005 Hydrates. Simulations of confined hydrates modeled with the TIP4P/2005 potential were run over the temperature range 200−310 K. These temperatures are higher than those used with the TIP4P potential because the TIP4P/2005 model has a higher bulk melting point. Methane loading data from these calculations are shown in Figure 5. Overall, these data are similar to those obtained with the TIP4P potential, only shifted to slightly higher temperatures. In all pore sizes and pressures, the hydrate cages are fully and singly occupied at 200 K except in the 0.5 u pore at 1 bar, where the cage occupancy is only 90%. At pressures of 10 and 100 bar, a sharp drop in loading, corresponding to decomposition, is observed at some temperature. However, at 1 bar, the desorption of methane occurs much more smoothly, again for all pore sizes. This differs from the behavior observed for the TIP4P hydrates, in which gradual desorption was only observed in the 2.0 u pore. In the TIP4P/2005 0.5 u system, Figure 5d, at 10 bar, the hydrate decomposes at 220 K, before sharp desorption, but at 1 bar at 210 K, after it. At 100 bar, the decomposition occurs at 240 K, after sharp desorption. Finally, methane loading data for the two offset structures are very nearly the same in all cases except, again, for the 100 bar data in the 1.0 u pore. As in the TIP4P case, the offset 2 structure here decomposes at a slightly higher temperature than the offset 1 structure.

Selected density and order parameter profiles for the 1.5 u system at 100 bar are given in Figure 6. The three temperatures at which data are shown correspond to the last three points in Figure 5b, that is, the sharp drop in n_{CH_4}. Between 290 and 300 K, the total methane loading decreases by 40%. By 310 K, methane desorbs completely from the interior of the pore, with significant density remaining only close to the walls (Figure 6a). The water density and order parameter profiles in Figure 6b show clearly that at 290 K the hydrate structure is well ordered. At 300 K, Figure 6c, the hydrate structure near one wall has decomposed, but the hydrate near the opposite wall remains well ordered. Either this simulation was insufficiently well equilibrated or the decomposition process was interrupted (on the simulation time-scale) by a kinetic barrier, perhaps at a particularly low-energy position of the liquid/hydrate interface. At 310 K, the cage structure has collapsed completely (Figure 6d). The hydrate decomposition temperature is therefore between 290 and 310 K, and most likely between 290 and 300 K. Corresponding simulation snapshots are shown in Figure 7, and confirm that the hydrate is well ordered at 290 K, partially decomposed at 300 K, and fully dissociated at 310 K. At 310 K, the density profile of water in the central part of the pore is smooth and near the corresponding bulk liquid value, though significant solvation structure is still evident near the walls. Interestingly, empty cages are not observed in this system at any temperature, indicating that the hydrate dissociation and methane desorption occur simultaneously. This is also true for the TIP4P/2005 hydrates at other pore sizes, and is qualitatively different than the case of TIP4P hydrates, where

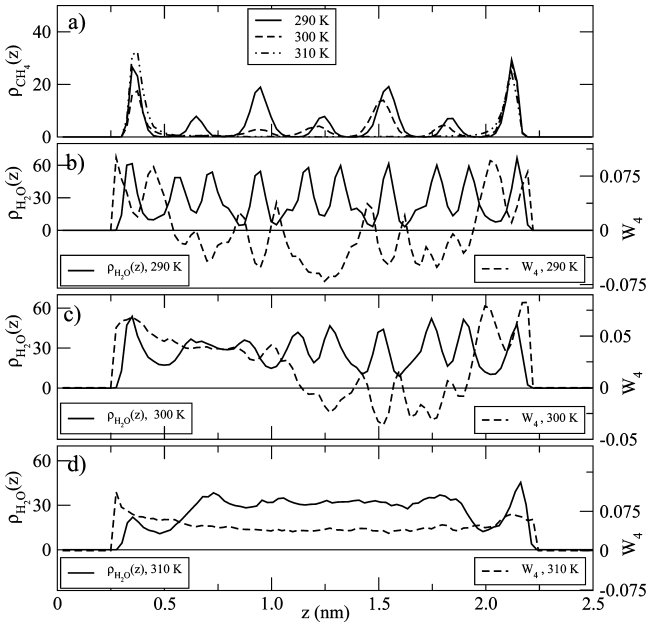

Figure 6. Density and order parameter profiles in the 1.5 u TIP4P/2005 hydrate at 100 bar: (a) methane density profiles at 290, 300, and 310 K; (b−d) density and order parameter profiles of water at (b) 290 K, (c) 300 K, and (d) 310 K.

we observed empty but stable hydrate cages prior to structural decomposition.

C. SPC/E Hydrates. Simulation results for confined SPC/E hydrates are shown in Figure 8. The SPC/E model has the lowest melting point of the water models used in this study, so these simulations were run over a lower temperature range than either of the TIP4P models. In the 2.0 u pore, Figure 8a, the methane data are qualitatively different than those of the TIP4P models. At all three pressures, a sharp drop is observed beginning at 180 K (1 bar) or 190 K (10 and 100 bar). These temperatures are much closer together than the corresponding decomposition temperatures in the TIP4P models. There are also significant differences in the methane loading data for the differently offset structures in the 2.0 u system, with offset 1 desorbing more sharply and at higher temperatures than offset 2. Analysis of density and order parameter profiles indicates that dissociation occurs at the start of methane desorption. This may explain the small rise in methane loading between 170 and 190 K at 100 bar; at 170 and 180 K, cages adjacent to the walls are quite disordered, permitting additional methane adsorption near the pore walls. In the 1.5 u hydrate, Figure 8b, decomposition again occurs prior to significant methane desorption, at 190 K at 1 bar, 200 K at 10 bar, and 210 K at 100 bar. Decomposition in the 1.5 u pore occurs at higher temperatures than in the 2.0 u pore. The 1.5 u isobars also display small increases in methane loading with increasing temperature but only after the sharp drop that follows dissociation; this is attributed to substantial rearrangement of the water structure. In the 1.0 u pore, Figure 8c, decomposition and substantial desorption occurs at yet higher temperatures than in the 1.5 u system. Very substantial differences between the two offsets are seen here, with offset 1 again stable to higher temperatures than offset 2 at all pressures. In the 0.5 u SPC/E system, Figure 8d, at 1 bar, the hydrate decomposes even at the lowest temperature studied; at higher pressures, the behavior is similar to that in larger pores. Interestingly, the identified 0.5 u

dx.doi.org/10.1021/jp205241n | J. Phys. Chem. B 2012, 116, 2183−2197

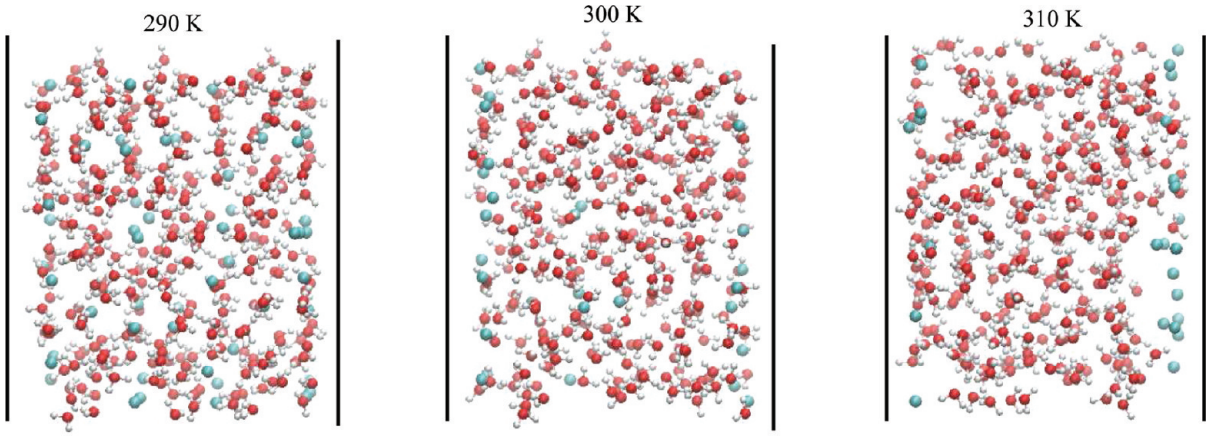

Figure 7. Simulation snapshots of the 1.5 u TIP4P/2005 hydrate at 100 bar and at 290, 300, and 310 K. The color scheme is the same as that in Figure 4.

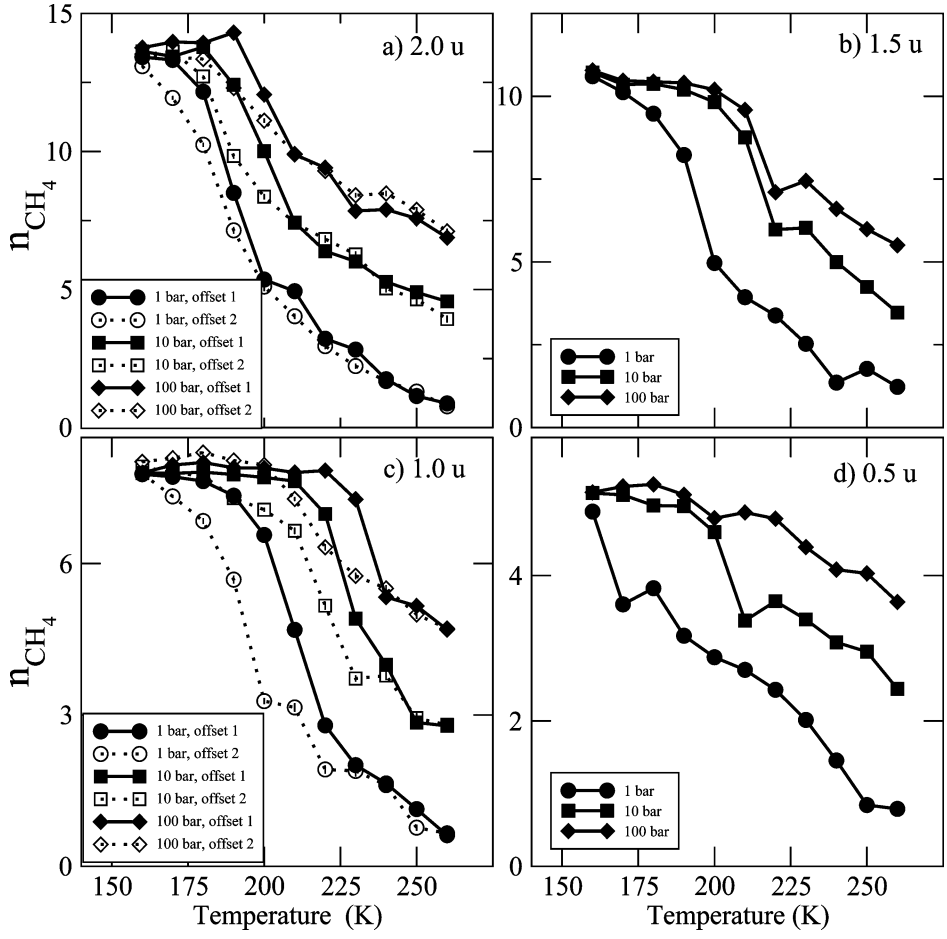

Figure 8. Methane loading data in systems modeled using the SPC/E potential; details as in Figure 2.

decomposition temperature of 200 K (at both 10 and 100 bar) is lower than in the 1.0 u pore, reversing the trend of higher stability in smaller pores in this system.

The SPC/E hydrate decomposition process is similar in all the pore sizes studied, so only the 1.0 u (offset 2) system at 1 bar is discussed in detail (Figure 9). At 180 and 190 K, methane density peaks are seen at characteristic positions across the pore, with only a 15% reduction in total loading by 190 K. From 190 to 200 K, total loading decreases by a further 40% and the methane density in the interior of the pore disappears entirely, indicating complete desorption from this region. Water density and order parameter profiles in Figure 9b and c clearly indicate that the clathrate structure largely collapses between 180 and 190 K, prior to substantial desorption. Simulation snapshots (Figure 10) show that at 180 K the crystal is well-formed and fully occupied, while at 190 K the structure close to the walls was completely disordered, but some cages are still visible in the center of the pore. In all pore sizes, snapshots of the fully decomposed SPC/E hydrates show that some regions near the pore walls are completely evacuated by water and filled

dx.doi.org/10.1021/jp205241n | J. Phys. Chem. B 2012, 116, 2183–2197

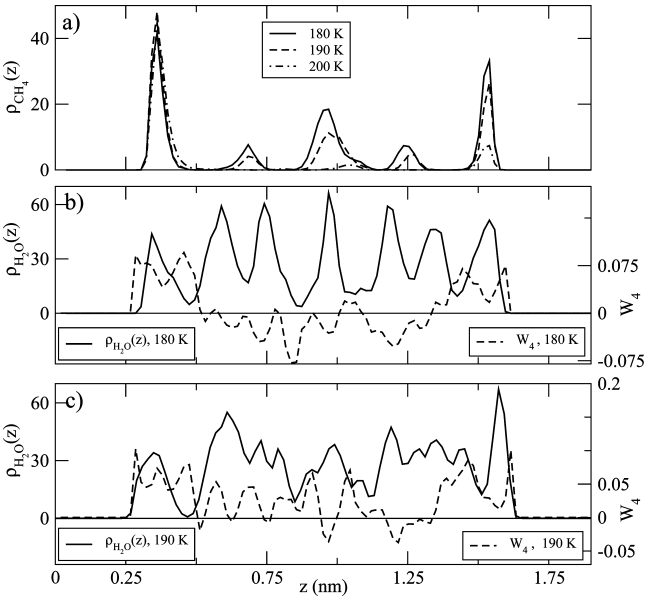

Figure 9. Density and order parameter profiles in the 1.0 u (offset 2) SPC/E hydrate at 1 bar: (a) methane density profiles at 180, 190, and 200 K; (b and c) density and order parameter profiles of water at (b) 180 K and (c) 190 K.

with methane, with vacant space visible in between. These regions are not uniformly distributed, suggesting glassy behavior consistent with the very low temperatures simulated. This leads to asymmetric distributions in methane density as observed in the 200 K data. The simulation snapshots (Figure 10) also show asymmetric distributions of methane at both 190 and 200 K, with methane strongly clustered at one pore wall.

D. Phase Diagrams and Dependence of Stability on Pore Size. For all systems, we determined the decomposition temperatures using methane desorption data, the density and order parameter profiles, and simulation snapshots. These results, discussed in part above, are collected in Table 2. The temperatures reported are the lower bound of the temperature interval over which decomposition occurs, equivalent to the highest temperature at which the hydrate is observed to be stable for the duration of the simulation. For example, for a hydrate stable at 200 K but decomposed at 210 K, the reported temperature is 200 K. In comparing two hydrates at the same pressure, we consider one to be the more stable if it decomposes at a higher temperature than the other.

In the TIP4P and TIP4P/2005 systems, at all pressures, the dissociation temperatures strictly increase with pore size. 2.0 u hydrates have the highest dissociation temperatures and 0.5 u hydrates the lowest. The difference in dissociation conditions of the two offset structures modeled using either of the TIP4P potentials is small, in all cases within 10 K, which is also the temperature resolution of the simulation protocol used.

As previously discussed, an inverse relationship between pore width and melting point is predicted by the Gibbs−Thomson equation. This clearly does not hold for the SPC/E hydrates. This proportionality is tested for the TIP4P and TIP4P/2005 hydrates in Figure 11 using data taken at 1 bar. We estimated the melting temperatures of the corresponding bulk hydrates, T_m(bulk), using simulation protocols similar to those applied to the confined systems. The TIP4P and TIP4P/2005 bulk hydrates were found to melt at 280 and 310 K, respectively. Again, these methods do not provide a "thermodynamic" melting point but instead measure the limit of stability under certain conditions. Nonetheless, because the same protocols were used for both the bulk and confined systems, the shifts in melting point due to confinement should be reasonably reliable; systematic errors will not affect this quantity as strongly as they would the absolute melting points. The resulting linearity of the shift in melting temperature with inverse pore width (Figure 11) indicates that the classically predicted behavior is displayed by both of these models, even in pores as small as 0.5 u, too narrow to contain even a single complete clathrate cage. The slopes associated with the two TIP4P-type models appear to be slightly different but cannot be reliably distinguished without more precise data.

The situation is very different for hydrates modeled using the SPC/E potential. At any pressure, the dissociation temperature of the 1.0 u offset 1 hydrate is the highest, followed by 1.5 u, 1.0 u offset 2, and the two 2.0 u hydrates (with nearly the same stability), in decreasing order. In addition, the two offset structures have substantially different stability. In order to better understand why this is the case, we considered

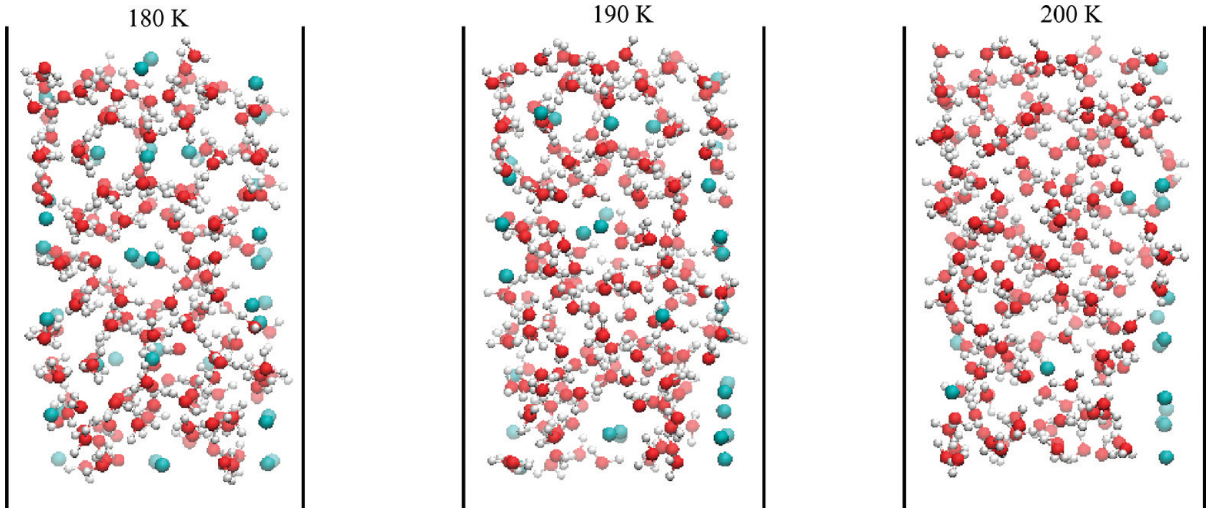

Figure 10. Simulation snapshots of the 1.0 u (offset 2) SPC/E hydrate at 1 bar and at 180, 190, and 200 K. The color scheme is the same as that in Figure 1.

dx.doi.org/10.1021/jp205241n | J. Phys. Chem. B 2012, 116, 2183−2197

Table 2. Hydrate Dissociation Temperatures from Isobaric Series Simulations[a]

		2.0 u		1.5 u	1.0 u		0.5 u
models	pressure (bar)	offset 1 (K)	offset 2 (K)	(K)	offset 1 (K)	offset 2 (K)	(K)
TIP4P	1	250	250	240	240	240	200
	10	270	270	260	250	250	220
	100	280	280	280	270	260	230
TIP4P/2005	1	280	280	260	250	240	210
	10	290	280	280	270	270	220
	100	300	300	290	280	290	240
SPC/E	1	180	170	190	200	180	unst
	10	190	180	200	220	210	200
	100	190	190	210	230	220	200

[a]Hydrates found to be unstable over the entire temperature range simulated are labeled "unst".

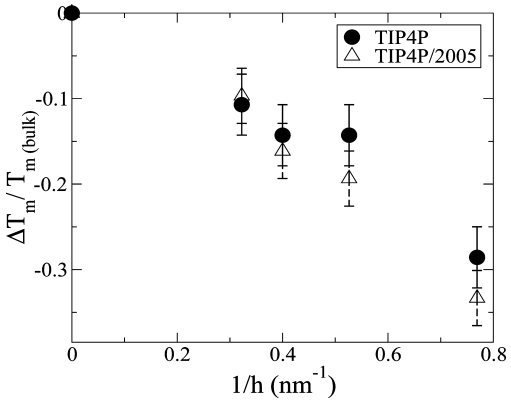

Figure 11. $\Delta T_m/T_{m(bulk)}$ vs inverse pore width, $1/h$.

components of the internal energies of 1.0 u hydrates at 190 K and 100 bar, shown in Table 3. For the TIP4P and TIP4P/2005 hydrates, the various terms are essentially identical for the differently offset structures. For the SPC/E hydrates, however, the Coulombic part of the energy of the offset 1 hydrate is lower than that of the offset 2 hydrate by ~1 kJ/mol of water. We hypothesize that this additional contribution stabilizes the offset 1 structure relative to the offset 2 structure. The source of this relative stabilization appears to be small relaxations of the hydrate crystal surfaces facing the pore walls; these components of the system energy are virtually identical for the differently offset unrelaxed (ideal) crystal structures.

IV. CONCLUSIONS

The stability of methane hydrates confined in very narrow slit-shaped pores has been studied using Monte Carlo simulations. Methane desorption and hydrate dissociation under conditions of increasing temperature at constant applied methane pressure are investigated in detail. These simulation conditions mimic those in a well-known experimental study,[16] in which a fixed amount of water was preadsorbed into a porous material and the temperature and applied methane pressure were systematically varied. Density and order parameter profiles of the hydrate components are shown to be useful analytical tools by which we can locate and explain changes in the state of confined hydrates.

At low temperatures, bulk-like hydrate structures were found to be stable in all pore sizes, at least for durations accessible to molecular simulation. At higher temperatures, the hydrates dissociate, after which methane occupies the region close to the walls, while water fills the interiors of the pore. Intermediate between the stable and decomposed hydrates, these systems displayed a variety of complex behaviors, as the partial desorption of methane from the clathrate cages and decomposition of the cages themselves are closely coupled.

Perhaps the most significant finding of this study is that, in hydrates described using TIP4P–type water models, Gibbs–Thomson-like behavior persists down to pore sizes smaller than a single clathrate cage. That is, the melting point depression due to confinement was found to be inversely proportional to the pore size, at least in the case of smooth-walled slit-pore geometries with pore sizes commensurate (or half-commensurate) with the crystal structure. Even in regular systems, below some pore width, hydrate-like structures must become unstable (eventually the system becomes effectively two-dimensional), but apparently pores small enough to contain only "half-cage" hydrate structures are still above that line. It is possible that in pores that cannot evenly incorporate half-integer numbers of hydrate unit cells anomalous behavior will be observed. Likewise, atomistically rough pore surfaces are likely to destabilize the confined hydrate crystal relative to the liquid phase, and further depress the melting temperature, though it is possible that Gibbs–Thomson behavior may still persist down to comparably small pores in such systems.

Table 3. Wall–Fluid, Fluid–Fluid, and Coulombic Components of the Average Potential Energy, from Simulations of two 1.0 u Offset Hydrates at 190 K and 100 bar[a]

	TIP4P		TIP4P/2005		SPC/E	
interaction	offset 1	offset 2	offset 1	offset 2	offset 1	offset 2
wall–H_2O	−2.31(12)	−2.30(13)	−2.56(13)	−2.56(14)	−2.26(14)	−2.16(15)
wall–CH_4	−6.54(11)	−6.55(12)	−6.57(4)	−6.63(5)	−6.61(8)	−6.41(9)
dispersion	6.82(14)	6.43(13)	7.47(13)	7.59(14)	7.74(11)	7.45(12)
Coulombic	−58.05(15)	−58.13(19)	−64.62(18)	−64.52(20)	−62.63(15)	−61.51(17)

[a]Wall–H_2O and Coulombic interactions are given per mole of water. Wall–CH_4 is given per mole of methane, and dispersion interactions are per mole of total adsorbate (methane + water). Uncertainties in the last digit(s) are given in parentheses.

dx.doi.org/10.1021/jp205241n | J. Phys. Chem. B 2012, 116, 2183–2197

The pores used here were substantially smaller than those considered in experimental studies to date and, as such, complement the existing experimental literature. As a result, substantially larger depressions of the freezing temperature were found (as much as 20% below the bulk hydrate melting temperature). In the systems studied here, the hydrate structures within approximately 5 Å of the pore wall tended to be rather disordered relative to the structure in the center of the pore, but no "liquid-like" layer was observed near the pore wall below the hydrate melting temperature, as claimed in experiments. It is likely that this is due to the use of smooth, parallel pore walls, which are known to enhance liquid packing and may preferentially stabilize well-ordered structures. Silica gels, in contrast, have surfaces quite rough on the atomic scale.

The different water models used in this study exhibited different behavior, which suggests that, at the very least, water models must be quite carefully chosen in future work on confined hydrate systems. Since the stability limits of the different models are themselves different, comparisons between them should be made not at the same absolute temperatures but at the same displacements relative to the observed transitions. The behavior and (relative) stability of the closely related TIP4P and TIP4P/2005 models were generally quite similar, although there were some minor differences observed. In particular, as the temperature is raised under quasi-equilibrium conditions, methane desorption tended to slightly precede collapse of the clathrate cage structure in the confined TIP4P hydrates, while in TIP4P/2005 hydrates these two processes were generally simultaneous. It would be difficult to meaningfully assign this difference in behavior to some particular difference between the potentials. The lower temperature of the TIP4P hydrate dissociation might contribute to the observed stability of the empty cages at that point, but the TIP4P hydrate is also less stable overall (the cause of the lower temperature), which would destabilize them. Finally, in both of the TIP4P models, the various "offset" structures generally had the same stability to within the precision of data obtained.

The SPC/E model behaved rather differently than the TIP4P models, in both quantitative and qualitative ways. Confined SPC/E hydrates were substantially less stable than bulk SPC/E water ice, which was not the case for the TIP4P hydrates. There was no clear dependence of confined SPC/E hydrate stability on pore size. Finally, when modeled with the SPC/E potential, the differently offset confined hydrate structures had significantly different stabilities, which is attributed to changes in the structure of the confined hydrates near the pore walls. The decomposed SPC/E clathrates displayed a somewhat glassy structure, which is probably related to the unrealistically low decomposition temperature of this model. Although SPC/E is widely regarded to be a good model for liquid water under near-ambient conditions, even small changes in an interaction potential can lead to large changes in phase boundaries, and since many fluid properties are strongly dependent on temperature, use of a model with a resonable melting point is recommended in studies of this type. It therefore appears likely that the TIP4P-type potentials are a more reliable choice for simulation of confined hydrates, as they display generally good qualitative agreement with experimental findings and much more reasonable stability limits. Only a single type of wall (graphite) was considered in this study, and there remains the possibility that the strange behavior of the SPC/E hydrates was in some way linked to the particular choice of surface–fluid interaction, but the unusually low melting point of this model is probably the underlying problem.

Through this work, we have shown that methane hydrates confined in porous media can be effectively treated using common water models and simulation techniques. These simulations aid in understanding confined hydrate equilibria and the effects of pore size on decomposition temperature. Some care is clearly required in choice of water models and in pore–fluid interaction potentials, as even relatively small changes appear to have substantial effects on observed behavior. Future simulation studies of these systems should include thermodynamic analysis based on calculation of the free energy of the confined hydrates, although such calculations are also subject to proper determination of the thermodynamically most stable crystal structure at low temperatures, and likely nonergodic behavior at higher temperatures. "Cooling" simulations, in which the temperature is lowered until clathrate crystals spontaneously form in the pores, would be desirable and would help understand hysteresis in these systems, but would also require very much longer simulations in order to obtain well-ordered crystals. We note that some recent progress in this direction has been made by Liang et al. in "steady-state" molecular dynamics simulations of the growth of hydrates confined between silica walls.[66] Finally, simulations that allow for realistic kinetics of transport of methane between the pores and bulk reservoir are desirable but, given the very long time-scales necessary for equilibration in experimental systems, may not be feasible on the molecular dynamics time-scale, instead requiring a kinetic Monte Carlo scheme or equivalent coarse-graining in time. Nonetheless, a detailed picture of nanoscale confined hydrate thermodynamics and kinetics does appear to be within reach.

■ ASSOCIATED CONTENT

Supporting Information

Selected plots of the energy and methane loading during the data collection phase. This material is available free of charge via the Internet at http://pubs.acs.org.

■ AUTHOR INFORMATION

Corresponding Author

*E-mail: lev.gelb@utdallas.edu.

■ ACKNOWLEDGMENTS

We acknowledge financial support from the National Science Foundation (CHE-0626008). Some of these calculations were performed on a computer system supported by an NSF CRIF award (CHE-0443511). Thanks also to Marcus G. Martin, author of MCCCS Towhee, for assistance with that simulation code.

■ REFERENCES

(1) Sloan, E. D. *Clathrate Hydrates of natural gases*; Marcel Dekker: New York, 1998.

(2) Buffett, B. A. Clathrate hydrates. *Annu. Rev. Earth Planet. Sci.* **2000**, *28*, 477–507.

(3) Koh, C. A. Towards a fundamental understanding of natural gas hydrates. *Chem. Soc. Rev.* **2002**, *31*, 157.

(4) Sloan, E. D. Fundamental principles and applications of natural gas hydrates. *Nature* **2003**, *426*, 353.

(5) Ripmeester, J. A.; Tse, J. S.; Ratcliff, C. I.; Powell., B. M. A new clathrate hydrate structure. *Nature* **1987**, *325*, 135.

(6) Udachin, K. A.; Ratcliff, C. I.; Ripmeester., J. A. A dense and efficient clathrate hydrate structure with unusual cages. *Angew. Chem., Int. Ed.* **2001**, *40*, 1303.
(7) McMullan, R. K.; Jeffrey, G. A. Polyhedral clathrate hydrates. IX. structure of ethylene oxide hydrate. *J. Chem. Phys.* **1965**, *42*, 2725.
(8) Henry, P.; Thomas, M.; Ben Clennell, M. Formation of natural gas hydrates in marine sediments 2. thermodynamic calculations and stability conditions in porous conditions. *J. Geophys. Res., [Solid Earth]* **1999**, *104*, 23005.
(9) Kvenvolden, K. A. Methane hydrate major reservoir of carbon in the shallow geosphere? *Chem. Geol.* **1988**, *71*, 41−51.
(10) Lee, S.; Seo, Y. Experimental measurement and thermodynamic modeling of the mixed CH_4+C_3H_8 clathrate hydrate equilibria in silica gel pores: Effects of pore size and salinity. *Langmuir* **2010**, *26* (12), 9742−9748.
(11) Bottero, I.; Otero Arean, C.; Armandi, M.; Bonelli, B.; Garrone, E. Synthesis and characterization of ordered porous carbons with potential applications as hydrogen storage media. *Microporous Mesoporous Mater.* **2007**, *103*, 150.
(12) Zheng, Z.; Xia, K.; Jiang, J.; Gao, Q.; Hu, Juan Enhanced room temperature hydrogen storage capacity of hollow nitrogen-containing carbon spheres. *Int. J. Hydrogen Energy* **2010**, *35*, 210.
(13) Leeb, Y.-S.; Kima, B-J; Parkc, S.-J. Novel porous carbons synthesized from polymeric precursors for hydrogen storage. *Int. J. Hydrogen Energy* **2008**, *33*, 2254.
(14) Tse, J. S.; Klein, M. L.; McDonald, I. R. Molecular dynamics studies of ice Ic and the structure I clathrate hydrate of methane. *J. Phys. Chem.* **1983**, *87*, 4198−4203.
(15) Tse, J. S. Dynamical properties and stability of clathrate hydrates. *Ann. N. Y. Acad. Sci.* **1994**, *715*, 187.
(16) Handa, Y. P.; Stupin, D. Thermodynamic properties and dissociation characteristics of methane and propane hydrates in 70 Å radius silica gel pores. *J. Phys. Chem.* **1992**, *96*, 8599.
(17) Uchida, T.; Ebinuma, T; Ishizaki, T. Dissociation condition measurements of methane hydrate in confined small pores of porous glass. *J. Phys. Chem. B* **1999**, *103*, 3659.
(18) Uchida, T.; Ebinuma, T.; Takeya, S.; Nagao, J.; Narita, H. Effects of pore sizes on dissociation temperatures and pressures of methane, carbon dioxide, and propane hydrates in porous media. *J. Phys. Chem. B* **2002**, *106*, 820.
(19) Seo, Y.; Lee, H.; Uchida, T. Methane and carbon dioxide hydrate phase behaviour in small porous silica gels: Three-phase equilibrium determination and thermodynamic modeling. *Langmuir* **2002**, *18*, 9164.
(20) Seshadri, K.; Wilder, J. W.; Smith, D. H. Measurements of equilibrium pressures and temperatures for propane hydrate in silica gels with different pore-size distributions. *J. Phys. Chem. B* **2001**, *105*, 2627.
(21) Anderson, R.; Llamedo, M; Tohidi, B.; Burgass, R. W. Characteristics of clathrate hydrate equilibria in mesopores and interpretation of experimental data. *J. Phys. Chem. B* **2003**, *107*, 3500.
(22) Clarke, M. A.; Darvish., M. P. A method to predict equilibrium conditions of gas hydrate formation in porous media. *Ind. Eng. Chem. Res.* **1999**, *38*, 2485.
(23) Wilder, J. W.; Sheshadri, K.; Smith, D. H. Modeling hydrate formation in media with broad pore size distributions. *Langmuir* **2001**, *17*, 6729.
(24) Klauda, J. B.; Sandler, S. I. Modeling gas hydrate phase equilibria in laboratory and natural porous media. *Ind. Eng. Chem. Res.* **2001**, *40* (20), 4197−4208.
(25) Alba-Simionesco, C; Coasne, B.; Dosseh, G.; Dudziak, G.; Gubbins, K. E; Radhakrishnan, R.; Sliwinska-Bartkowiak, M. Effects of confinement on freezing and melting. *J. Phys.: Condens. Matter* **2006**, *18* (6), R15−R68.
(26) Miyahara, M.; Gubbins, K. E. Freezing/melting phenomena for Lennard-Jones methane in slit pores: A monte carlo study. *J. Chem. Phys.* **1997**, *106* (7), 2865−2880.
(27) English, N. J.; MacElroy, J. M. D. Structural and dynamical properties of methane clathrate hydrates. *J. Comput. Chem.* **2003**, *24*, 1569−1581.
(28) Chialvo, A. A.; Houssa, M.; Cummings, P. T. Molecular dynamics study of the structure and thermophysical properties of model sI clathrate hydrates. *J. Phys. Chem. B* **2002**, *106*, 442−451.
(29) Okano, Y.; Yasuoka, K. Free-energy calculation of structure-H hydrates. *J. Chem. Phys.* **2006**, *124*, 024510-1−024510-9.
(30) Vatamanu, J.; Kusalik, P. G. Unusual crystalline and polycrystalline structures in methane hydrates. *J. Am. Chem. Soc.* **2006**, *128*, 15588−15589.
(31) Katsumas, K.; Koga, K.; Tanaka, H. On the thermodynamic stability of hydrogen clathrate hydrates. *J. Chem. Phys.* **2007**, *127*, 044509−1.
(32) Alavi, S.; Ripmeester, J. A.; Klug, D. D. Molecular dynamics study of the stability of methane structure H clathrate hydrates. *J. Chem. Phys.* **2007**, *126*, 124708-1−124708-6.
(33) Moon, C.; Hawtin, R. W.; Rodger, P. M. Nucleation and control of clathrate hydrates: insights from simulation. *Faraday Discuss.* **2007**, *136*, 367−382.
(34) Wierzchowski, S. J.; Monson, P. A. Calculation of free energies and chemical potentials for gas hydrates using monte carlo simulations. *J. Phys. Chem. B* **2007**, *111*, 7274−7282.
(35) Jiang, H.; Jordan, K. D.; Taylor, C. E. Molecular dynamics simulations of methane hydrate using polarizable force fields. *J. Phys. Chem. B* **2007**, *111*, 6486−6492.
(36) Walsh, M. R.; Koh, C. A.; Sloan, E. D.; Sum, A. K.; Wu, D. T. Microsecond simulations of spontaneous methane hydrate nucleation and growth. *Science* **2009**, *326*, 1095−1098.
(37) Forrisdahl, O. K; Kvamme, B.; Haymet, A. D. J. Methane clathrate hydrates: melting, supercooling and phase separation from molecular dynamics computer simulations. *Mol. Phys.* **1996**, *89*, 819.
(38) Mastny, E. A.; Miller, C. A.; de Pablo, J. The effect of the water/methane interface on methane hydrate cages: The potential of mean force and cage lifetimes. *J. Chem. Phys.* **2008**, *129*, 034701.
(39) Sun, R.; Duan, Z. Prediction of CH_4 and CO_2 hydrate phase equilibrium and cage occupancy from ab initio intermolecular potentials. *Geochim. Cosmochim. Acta* **2005**, *69*, 4411.
(40) Sizov, V. V.; Piotrovskaya, E. M. Computer simulation of methane hydrate cage occupancy. *J. Phys. Chem. B* **2007**, *111*, 2886.
(41) Rodger, P. M. Simulations of the methane hydrate/methane gas interface near hydrate forming conditions conditions. *Fluid Phase Equilib.* **1996**, *116*, 326.
(42) Berendsen, H. J. C.; Grigera J, R.; Straatsma., T. P. The missing term in effective pair potentials. *J. Phys. Chem.* **1987**, *91*, 6269.
(43) Jorgensen, W. L.; Chandrasekhar, J.; Madura, J. D.; Impey, R. W.; Klein, M. L. Comparison of simple potential functions for simulating liquid water. *J. Chem. Phys.* **1983**, *79*, 926.
(44) Sanz, E.; Vega, C.; Abascal, J. L. F.; MacDowell, L. G. Phase diagram of water from computer simulation. *Phys. Rev. Lett.* **2004**, *92* (25), 255701.
(45) Abascal, J. L. F.; Vega., C. A general purpose model for the condensed phases of water: TIP4P/2005. *J. Chem. Phys.* **2005**, *123*, 234505.
(46) Docherty, H.; Galindo, A; Vega, C.; Sanz., E. A potential model for methane in water describing correctly the solubility of the gas and the properties of the methane hydrate. *J. Chem. Phys.* **2006**, *125*, 074510.
(47) Jorgensen, W. L.; Madura, J. D.; Swenson, C. J. Optimized intermolecular potential functions for liquid hydrocarbons. *J. Am. Chem. Soc.* **1984**, *106*, 6638.
(48) Lorentz, H. A. Ueber die anwendung des satzes vom virial in der kinetischen theorie der gase. *Ann. Phys.* **1881**, *248*, 127−136.
(49) Berthelot, D. C. R. *Acad. Sci. Paris* **1898**, *126*, 1703.
(50) Vega, C.; Docherty, H.; Galindo, A.; Sanz, E. A potential model for methane in water describing correctly the solubility of the gas and the properties of the methane hydrate. *J. Chem. Phys.* **2006**, *125*, 074510.

(51) Miyahara, M.; Gubbins, K. E. Freezing/melting phenomena for Lennard-Jones methane in slit pores: A monte carlo study. *J. Chem. Phys.* **1997**, *106*, 2865.
(52) Radhakrishnan, R.; Trout., B. L. A new approach for studying nucleation phenomena using molecular simulations: Application to CO_2 hydrate clathrates. *J. Chem. Phys.* **2002**, *117*, 1786.
(53) Gelb, L. D.; Gubbins, K. E.; Radhakrishnan, R.; Sliwinska-Bartkowiak, M. Phase separation in confined systems. *Rep. Prog. Phys.* **1999**, *62*, 1573−1659.
(54) W. A. Steele. *The interaction of Gases with solid surfaces*; Pergamom Press: Oxford, U.K., 1974.
(55) Bernal, J. D.; Fowler., R. H. A theory of water and ionic solution, with particular reference to hydrogen and hydroxyl ions. *J. Chem. Phys.* **1933**, *1*, 515.
(56) Buch, V.; Sandler, P.; Sadlej, J. Simulations of H_2O solid, liquid, and clusters, with an emphasis on ferroelectric ordering transition in hexagonal ice. *J. Phys. Chem. B* **1998**, *102*, 8641.
(57) Krichner, M. T.; Boese, R.; Billups, W. E.; Norman, L. R. Gas hydrate Single-Crystal structure analyses. *J. Am. Chem. Soc.* **2004**, *126*, 9407.
(58) Kang, S.; Lee, J.; Ryu, H. J. Phase behavior of methane and carbon dioxide hydrates in meso- and macro-sized porous media. *Fluid Phase Equilib.* **2008**, *274*, 68.
(59) Martin M. http://towhee.sourceforge.net/.
(60) McEnaney, B.; Mays, T. J.; Rodrguez-Reinoso, F. Fundamental aspects of active carbons. *Carbon* **1998**, *36* (6).
(61) Müller, E. A.; Rull, L. F.; Vega, L. F.; Gubbins, K. E. Adsorption of water on activated carbons: A molecular simulation study. *J. Phys. Chem.* **1996**, *100*, 1189−1196.
(62) Flyvbjerg, H.; Petersen, H. G. Error estimates on averages of correlated data. *J. Chem. Phys.* **1989**, *91*, 461.
(63) Steinhardt, P. J.; Nelson, D. R.; Ronchetti, M. Bond-orientational order in liquids and glasses. *Phys. Rev. B* **1983**, *28*, 784.
(64) Liua, C.-J.; Guo, G.-J.; Zhang, Y.-G.; Li., K.-H. Using the face-saturated incomplete cage analysis to quantify the cage compositions and cage linking structures of amorphous phase hydrates. *Phys. Chem. Chem. Phys.* **2011**, *13*, 12048.
(65) Heffelfinger, G. S.; van Swol, F. Diffusion in lennard-jones fluids using dual control volume grand canonical molecular dynamics simulation (dcv-gcmd). *J. Chem. Phys.* **1994**, *100*, 7548.
(66) Liang, S.; Rozmanov, D.; Kusalik, P. G. Crystal growth simulations of methane hydrates in the presence of silica surfaces. *Phys. Chem. Chem. Phys.* **2011**, *13*, 19856−19864.